

Supporting Information for

# Genetically encoded phase contrast agents for digital holographic microscopy

Arash Farhadi,<sup>†,‡</sup> Manuel Bedrossian,<sup>‡,‡</sup> Justin Lee,<sup>†</sup> Gabrielle H. Ho,<sup>¶</sup> Mikhail G. Shapiro,<sup>\*,¶</sup> Jay L. Nadeau<sup>\*,§</sup>

<sup>†</sup> Division of Biology and Biological Engineering, California Institute of Technology, Pasadena, CA USA

<sup>‡</sup> Division of Engineering and Applied Science, California Institute of Technology, Pasadena, CA USA

<sup>¶</sup> Division of Chemistry and Chemical Engineering, California Institute of Technology, Pasadena, CA USA

<sup>§</sup> Department of Physics, Portland State University, Portland, OR USA

<sup>‡</sup> Contributed equally

\*Correspondence should be addressed to M.G.S. (mikhail@caltech.edu) or J.N. (nadeau@pdx.edu)

## **This PDF file includes:**

Materials and Methods  
Supplementary text  
Figs. S1 to S3  
Table S1  
Captions for datasets S1 to S9  
References for SI reference citations

## **Other supplementary materials for this manuscript include the following:**

Datasets S1 to S9

## Supporting Information Text

### Materials and Methods

#### Digital Holographic Microscopy

Two instruments were used: a “high power” instrument and a “low power” instrument. The design of the “high power” microscope was a modified Mach-Zehnder as described previously,<sup>1</sup> containing identical objective lenses in the object and reference beams. The objective lenses used were Mitotoyo 100x, NA 0.7 dry long working distance objectives, infinity-corrected to an achromatic field lens (200 mm focal length), which was used to form the image on a digital CCD camera (Baumer TXG50-P). The effective magnification of this instrument was 78x. The diffraction-limited lateral resolution was roughly 0.3  $\mu\text{m}$  with a 405 nm illumination source. Illumination was through a single-mode fiber coupled diode laser that was collimated before the first beamsplitter.

The design of the “low power” microscope was a common path Mach-Zehnder as described previously.<sup>2,3</sup> The objectives were simple aspheric lenses (Asphericon) with NA = 0.3. The effective magnification was 19.6x with a diffraction limited lateral resolution of 0.8  $\mu\text{m}$ . The wavelength used in this work for both DHM instruments was 405 nm, supplied by a diode laser (Thorlabs S1FC405).

DHM images of GV-labeled mammalian cells were acquired using the “high power” microscope and all other DHM data were collected using the “low power” microscope.

#### Gas Vesicle Expression, Purification, and Clustering

*Anabaena flos-aquae* (CCAP strain 1403/13F) was cultured for ~2 weeks in Gorham’s media supplemented with BG-11 solution (Sigma) and 10 mM  $\text{NaHCO}_3$  at 25°C, 100 rpm under 1%  $\text{CO}_2$  and a 14 hours light/10 hours dark cycle.<sup>4</sup> At confluency, the buoyant cell fraction was isolated by floating to the top of a separating funnel over a 48h period, after which the supernatant was discarded. The collected cells were then lysed using 500 mM sorbitol and 10% Solulyse solution (Genlantis). GVs were purified through repeated rounds of isolating the buoyant fraction through centrifugation and resuspension in PBS.

GV clusters were prepared by first biotinylating purified GVs with  $10^5$  molar excess of EZ-Link Sulfo-NHS-LC-biotin (Thermo Scientific) in PBS for 4 hours. Afterwards, the sample underwent two rounds of overnight dialysis in PBS. The biotinylated GVs were then clustered by incubation with streptavidin (Geno Technology) for 30 minutes at room temperature at a streptavidin to GV molecular ratio of 100:1.

#### Dynamic Light Scattering (DLS)

The hydrodynamic size of the GVs, GV clusters and alumina beads was measured in 50  $\mu\text{L}$  samples at  $\text{OD}_{500} = 0.2$  using a Zeta-PALS analyzer (Brookhaven Instruments). Samples were mixed thoroughly and measured five times for each reported hydrodynamic diameter.

## Engineered Gas Vesicles for Cell Labeling

Genetically engineered GvCs were prepared using a previously described protocol.<sup>5</sup> In brief, the GvpC DNA sequence from *Anabaena flos-aquae* was codon-optimized for *E. coli* expression and cloned into a pET28a(+) plasmid (Novagen) with an N-terminal hexahistidine-tag and C-terminal GSGRRRRRRR (R8) sequence. Plasmids were transformed into BL21(DE3) cells (Invitrogen), which were induced to express the recombinant GvpC for 6 hours at 30°C. GvpC contained in inclusion bodies was purified by lysing the cells using 10% Solulyse (Genlantis) supplemented with DNaseI (10 µg/mL) and lysozyme (400 µg/mL) at room temperature. Inclusion bodies were recovered by centrifugation at 27,000g for 15 min. The inclusion body pellets were resuspended in 20 mM Tris-HCl buffer with 500 mM sodium chloride and 6 M urea (pH=8.0) and incubated with Ni-NTA resin (Qiagen, Valencia, CA) for 2 hours at 4°C. After washing, proteins were eluted using 250 mM imidazole.

Next, the wild-type GvpC proteins on the surface of GVs were replaced with polyarginine modified-GvpC (R8-GvpC). Purified GVs were treated with 6 M urea and 20 mM Tris-HCl (pH=8.0) to remove their wild-type GvpC. These stripped GVs were isolated with two rounds of centrifugally assisted buoyancy purification in urea. Purified R8-GvpC was then added according to the formula:  $2 \times \text{optical density} \times 198 \text{ nM} \times \text{liters GVs} = \text{nmol of recombinant GvpC}$  and dialyzed in PBS for 8 hours.  $10^5$  molar excess of Alexa Fluor 488 NHS (Thermo Fisher) was then added to the GVs and incubated at room temperature for 4 hours under gentle rotation, before being quenched with 20 mM Tris-HCl (pH = 8.0) and dialyzed in PBS to remove excess dye.

## Cell Culture and Gas Vesicle Labeling

Chinese hamster ovary cells (CHO-K1; ATCC) were cultured in DMEM (Corning) with 10% FBS (Thermo Fisher) and penicillin/streptomycin (Corning). Coverslips (18x18 mm) were sterilized with 70% ethanol, washed twice in PBS and placed in 6-well plates. Fibronectin (Sigma) was diluted 1:20 in PBS and 200 µL were added to each well over the entire surface of the coverslip and incubated for 1 hour at room temperature. Excess solution was aspirated, and CHO-K1 cells were seeded on the coverslips and grown to ~75% confluency.

For GV labeling, the surface of a 6-well plate was covered with paraffin and UV sterilized. Then, 300 µL of 37°C DMEM media and 300 µL of 114 pM (36.6 µg/mL or  $OD_{500} = 1$ ) of R8-GVs was added to the bottom of the well and mixed. The cells cultured on coverslips were inverted onto the DMEM and GV mixture, so the cells were facing the bottom of the plate. The coverslips and GVs were incubated at 37°C. Following incubation, the cells were washed three times with 200 µL of PBS and fixed with 1 mL of formaldehyde for 30 minutes. The coverslips were mounted using Diamond Antifade mountant (Thermo Fisher) and sealed using clear nail polish.

## Fluorescence Imaging

Fluorescence images were taken on an Olympus IX-71 inverted microscope using Hg lamp illumination through a 1.4 NA oil immersion objective and using the enhanced green fluorescent protein filter set (Chroma). To register fluorescence images with phase

images, a 1- $\mu\text{m}$  tip glass pipette was secured to the specimen and cells were imaged in the vicinity of the tip across the two instruments.

### **Gas Vesicle Expression in *Salmonella***

GV expression in *Salmonella typhimurium* (strain ELH1301) cells was performed as described previously.<sup>6</sup> Briefly, the hybrid GV gene cluster, under the control of the *luxI* promoter (Addgene 106475), was transformed into *S. typhimurium* cells. Monoclonal cells from an individual plated colony were cryostocked. Cells containing the GV genes were grown in 5 mL of 2xYT media with 50  $\mu\text{g}/\text{mL}$  kanamycin for 16 hours at 37°C, 250 rpm. Cultures in 50 mL 2xYT media with 50  $\mu\text{g}/\text{mL}$  kanamycin were then inoculated with 500  $\mu\text{L}$  of the starter culture and grown on the shaker at 37°C until  $\text{OD}_{600} = 0.4$  to 0.6. These cultures were induced with 3 nM *N*-( $\beta$ -ketocaproyl)-L-homoserine lactone (AHL) and then grown for 22 hours at 30°C, 250 rpm. Cells were then harvested by centrifugation at 300g at 30°C for 2 hours. The buoyant cell fraction was transferred into clean tubes. To collapse the GVs inside cells, GV-expressing salmonella were placed in a quartz cuvette (Hellma Analytics) connected to a  $\text{N}_2$  cylinder through a pressure controller (Alicat Scientific) set to 1.2 MPa.

### **TEM Sample Preparation and Imaging**

Electron microscopy was performed at the Beckman Institute Resource Center for Transmission Electron Microscopy at Caltech. Purified GVs were diluted to  $\text{OD}_{500} = 0.2$  in 10 mM HEPES buffer and *Salmonella* cells were diluted to  $\text{OD}_{600} \sim 0.2$  in 10 mM HEPES buffer or PBS. Samples were then spotted on Formvar/Carbon 200 mesh grids (Ted Pella), which were rendered hydrophilic by glow discharging (Emitek K100X). Purified GV samples were stained with 2% uranyl acetate, while cells were imaged unstained. Image acquisition was performed using a Tecnai T12 Lab6 120 kV transmission electron microscope equipped with a Gatan Ultrascan 2k x 2k CCD camera.

### **Simulations**

Holograms were simulated with MATLAB (R2017b) using a custom hologram simulation routine. First, a two-dimensional projection image was created using a series of Radon Transforms, modeling a typical GV-expressing *Salmonella* cell as a cylinder, with a diameter of 1  $\mu\text{m}$  and a length of 5  $\mu\text{m}$ , with bands of lower refractive index corresponding to areas dense in GVs as seen in TEM images. This projection is then downsampled, via bicubic interpolation, in order to accommodate and emulate the diffraction limited resolution of the low-power DHM instrument. Within this projection, GVs were simulated using index of refraction values of 1.00. Other intracellular areas were simulated using an index of refraction of 1.37. The index of refraction used to simulate the cell's surrounding medium is 1.33.

The wavefront perturbations as a result of a collimated plane wave passing through the simulated cell is then propagated using the angular spectrum method.<sup>7</sup> The resulting diffracted wavefront is numerically propagated and recombined with a reference (undisturbed) plane wave in order to simulate an off-axis hologram. Code for the simulator is provided in the Supplemental Material. The simulated holograms were reconstructed into phase images using the commercially available software KOALA (LynceeTec). No image noise was added to the simulation besides quantization noise

when the holograms were saved as unsigned 8-bit image files whereas in reality there are numerous sources of noise including, but not limited to: shot noise, temporal and spatial noise due to changes in the coherence of the illumination laser, as well as various sources of noise introduced by the digital CCD used to record the holograms.<sup>8</sup>

### **Tracking**

Tracking of GVs and alumina beads was performed using the Manual Tracking plug-in in the open source image analysis tool FIJI.<sup>9</sup>

### **Phase Quantification of *Salmonella* Cells**

Data recorded using the DHM system was reconstructed into phase images using the commercially available software Koala (LynceeTec). Raw 8-bit phase images were reconstructed with quantitative phase bounds of  $-\pi$  to  $\pi$  corresponding to pixel values of 0 and 255, respectively (described in supplementary text). After reconstruction cell boundaries were identified with the freehand selection tool of the open source image analysis software FIJI by team members blinded to the identity of the sample. The cell boundaries were used to isolate the interior pixel values within the cell by creating a binary mask about the cell boundary. These interior pixel values were converted from their 8-bit values to quantitative phase values and analyzed using MATLAB (2017b).

### **Image Processing and Handling**

In the analysis of off-axis holograms, image reconstruction and post-processing steps are necessary in order to interpret the electric field intensity recorded in a hologram into a useful three-dimensional data set. Furthermore, post-processing methods are used to de-noise the resulting reconstructed images.

This supplemental document outlines the methods and work flows associated with the processing and handling of off-axis holographic images. This includes the reconstruction process from hologram to phase images, and all de-noising steps used to reach the final images that are presented in the main document.

### Image Reconstruction

An off-axis hologram is recorded as a single image that contains interference patterns (or fringes) that contain the 3D information of the sample being imaged. The spatial frequency of the fringes act as the carrier frequency of this information. To reconstruct this information into a useable form, the high spatial frequency information in the hologram must be isolated. **Figure S1A** shows an example hologram, its Fourier Transform plotted on a logarithmic scale (note the high frequency ‘lobes’ which contain the 3D information of the sample (**Figure S1B**), the same Fourier transform that has been multiplied by a binary mask to isolate one of the high frequency lobes (**Figure S1C**), and that isolated lobe that has been shifted to the center of the Fourier Transform (**Figure S1D**).

In the formation of an off-axis hologram, two collimated beams of light are recombined at the digital detector at an angle (off-axis of each other). This off-axis recombination causes interference between the two beams. The spatial frequency of these

fringes is proportional to the wavelength of light used as well as the recombination angle. If the two beams of light are named the ‘specimen’ and ‘reference’ beam where the ‘specimen’ beam interacts with the sample being imaged, and the ‘reference’ beam remains undisturbed, then the resulting hologram can be represented mathematically as the superposition of the two beams at the detector (Equation 1).

$$S(x, y) = A_S \exp i(\phi_S(x, y) - \omega t), \quad 1a$$

$$R(x, y) = A_R \exp i(\phi_R(x, y) - \omega t), \quad 1b$$

$$\Psi(x, y) = S(x, y) + R(x, y), \quad 1c$$

$$h = \int \Psi\Psi^* dt = (I_S + I_R) + SR^* + S^*R, \quad 1d$$

where  $A_S$  and  $A_R$  are the amplitudes of the Specimen and Reference beam,  $\phi_S$  and  $\phi_R$  are the phase differences between the specimen and reference beams,  $\Psi$  is the resulting wave from the superposition of the specimen and reference beams, and  $h$  is the hologram.

In Supplementary Figure 1B there are three discrete lobes present. The center most lobe corresponds to the summation of intensities of the specimen and reference beams ( $I_S + I_R$ ) from Equation 1d, while the two higher spatial frequency lobes correspond to  $SR^*$  and  $S^*R$  from Equation 1d. These two lobes are complex conjugates of each other, but for the purposes of this work, the lobe corresponding to  $SR^*$  is the chosen lobe to be isolated in **Figure S1C & S1D**.

With the 3D information encoded in the hologram isolated, it is then convolved with the transfer function of free space ( $G$ ), according to Rayleigh-Sommerfeld diffraction, as described by Schnars, et al.<sup>7</sup> The reconstructed complex wavefront  $\Gamma$  is

$$\Gamma(x, y, z, t) = \mathfrak{F}^{-1}[\mathfrak{F}(h(x, y, t)) * G(f_x, f_y, z)], \quad 2a$$

$$G(f_x, f_y, z) = \exp\left\{\frac{-2\pi iz}{\lambda} \sqrt{1 - \lambda^2 f_x^2 - \lambda^2 f_y^2}\right\}, \quad 2b$$

$$I(x, y, z, t) = |\Gamma(x, y, z, t)|^2, \quad 2c$$

$$\phi(x, y, z, t) = \arctan\left(\frac{\Im(\Gamma(x, y, z, t))}{\Re(\Gamma(x, y, z, t))}\right), \quad 2d$$

where  $\mathfrak{F}$  is the Fourier Transform operator, the intensity image ( $I$ ) is calculated as the square of the magnitude of the complex wavefront  $\Gamma$ , and the quantitative phase image ( $\phi$ ) is defined as the inverse tangent of the imaginary parts of  $\Gamma$  divided by the real parts of  $\Gamma$ . The function  $G$  is a pure phase object that describes the propagation of an electric field through the focal plane ( $z$ ) and can be modulated to calculate the reconstructed wavefront throughout an entire volume. For a more in-depth derivation of this function, see Schnars, et al.<sup>7</sup>

### Post-Processing

With the reconstructed intensity  $I(x, y, z, t)$ , and phase images  $\phi(x, y, z, t)$ , post-processing is necessary to eliminate noise from various sources including, but not limited to, photon/shot noise, speckle noise, digitization noise, as well as detector noise. In addition, low spatial frequency artifacts are also common in phase reconstructions due to tilt in the sample chamber relative to the optical axis as well as objective lens curvature.

To remove as much noise from the reconstructed images as possible, temporally averaged images are calculated and subtracted from each phase image, as well as conducting spatial frequency band-pass filtering.

In the subtraction of temporally averaged phase (referred to as ‘mean subtraction’), the mean of each pixel is calculated through time. This mean image is then subtracted from the image used to calculate that mean. This effectively removes any stationary artifacts from the image highlighting any transient particle in the image.

After this mean subtraction, band-pass filtering is done to remove any low and high spatial frequency noise from the images. Low spatial frequency noise can be caused by tilt in the sample chamber relative to the optical axis, as well as by the curvature of the lenses used in the DHM instrument. Because the DHM is an instrument that is capable of achieving diffraction limited resolution, there is a physical limit of the spatial frequencies that can be recorded. This presents a clear upper limit to the spatial frequencies that carry useful information in the image. Any higher frequency artifacts in the image are by definition pure noise and are filtered out.

Because the phase images obtained using off-axis DHM are of a quantitative nature, this is the extent of the post-processing performed in order to preserve the quantitative information contained in the image. Other methods are more useful in enhancing contrast and suppressing noise but were not performed in this work.

### **Hologram Simulator**

The optical theory used in the MATLAB code discussed in this document are well reviewed by Ulf Schnars, et al.<sup>7</sup>. The main function (‘OAhologramSimulator.m’) expects as an input, two variables. The first is called ‘waveFront’. This is a complex matrix of the size of the final image. This matrix describes the normalized amplitude and phase of the electric field of the sample we wish to simulate. For the purposes of this manuscript, the variable ‘waveFront’ is provided in the file ‘waveFront.mat’. The second input variable is ‘desiredFileName’, which is the desired file path and name of the output. The output is the final 8-bit TIFF hologram.

The variable ‘waveFront’ is generated by creating two three dimensional matrices of the electric field attenuation and the index of refraction of light that passes through a cylindrical simulated ‘salmonella cell’ with the morphology as shown in the main manuscript.

With the two 3D matrices, a series of radon transforms are used to project a collimated beam of light through the object. These projections are then used to calculate the resultant wave front as a result of the projected electric field attenuation and phase delay (introduced by the index of refraction matrix). The hologram simulation code can be separated and described in eight sections.

## 1 DHM Parameters

This section establishes the optical performance parameters of the DHM instrument that is to be simulated. In this implementation, the off-axis holograms that are being simulated are of the ‘low-power’ instrument and have the appropriate performance parameters for that instrument.

Note that the numerical aperture of the objective lenses is not necessary because the geometric properties of the objective lens is inputted as ‘fl’ and ‘DiaLens’ (lens focal length and lens diameter, respectively).

## 2 Create the undisturbed reference beam

This section creates the reference wave. The reference wave by definition is undisturbed and un-attenuated and thus the reference wave is a simple matrix of ones.

## 3 Propagate target and ref to lens object focal plane

This section takes the input variable ‘waveFront’ and the newly created reference wave front ‘U2ref’ and propagates the two waves to the focal plane of the objective lens. The propagation of the two waves is conducted using the Angular Spectrum Method (ASM) as described in Schnars, et al. The propagation is done by calling an external function ‘ang\_spec\_prop.m’. The output of this section are the variables ‘U3’ and ‘U3ref’, corresponding to the propagated wave front of the sample (U3) and reference (U3ref).

## 4 Propagate to the lens

This section takes the output from the previous section and propagates the two wave fronts to the objective lens. This section uses the same external function as the previous section. The outputs are ‘U4’ and ‘U4ref’.

## 5 Simulate the phase delay introduced by the lens

This section models an ideal objective lens that introduces a phase delay into light as it travels through the lens. This simulates an ideal lens because it introduces no wave front aberrations or electric field attenuation.

In addition to simulating the phase delay caused by the objective lens, it applies this phase delay to ‘U4’ and ‘U4ref’. The output of this section is ‘Alens’ and ‘Alensref’.

## 6 Propagate to focal plane

This section takes the output of the previous section and propagates the two wave fronts to the back focal plane of the objective lens. The outputs of this section are the variables ‘U5’ and ‘U5ref’.

## 7 Combine wavefront with reference wave

This section acts as the relay lens of the ‘low-power’ instrument by recombining the object wave front (U5) with the reference wave front (U5ref) as well as introducing a tilt angle between them so that they create interference patterns at the ‘detector’. The output of this section becomes a single complex wave front ‘Uccd’.



### 8 Generate and save the hologram

Because optical detectors such as CCD's only image electric field intensities, the intensity of 'Uccd' is calculated and saved as an 8-bit TIFF image with the file path and location inputted at the very beginning of this routine.

### **3D Pseudo-Colored Rendering**

The 3D rendering was generated using the commercially available software ARIVIS Vision4D. This software allows the import of a multidimensional image that is to be visualized in a variety of ways. The 2D images that comprise the 3D image stack used in ARIVIS were first processed using the methods described in the Image Processing & Handling section of this document. These processed images were then thresholded using a user defined threshold. Next the magnitude of the image gradient was calculated and stored as a separate stack of 2D images. The two 3D image stacks were then imported to ARIVIS Vision4D. The pixel values were plotted using a pseudo-colored lookup table. The opacity of each pixel was plotted as a weighted function of the magnitude of the image gradient at that pixel. This was done to highlight areas of large changes in phase signal within the cell.

### **Author Contributions**

AF, MB, MGS, and JN conceived and planned the research. AF, JL and GH prepared the biological samples. MB and JN conducted the DHM data collection and reconstruction with help from AF. MB carried out the generation and analysis of the salmonella hologram simulations as well as the analysis particle and salmonella image reconstruction and data analysis. MB performed the processing and rendering of the 3D pseudo-colored phase image of CHO cells. AF, MB, MGS, JL, GH and JN analyzed the results. AF, MB, MGS and JN wrote the manuscript with input from all authors. MGS and JN supervised the research.

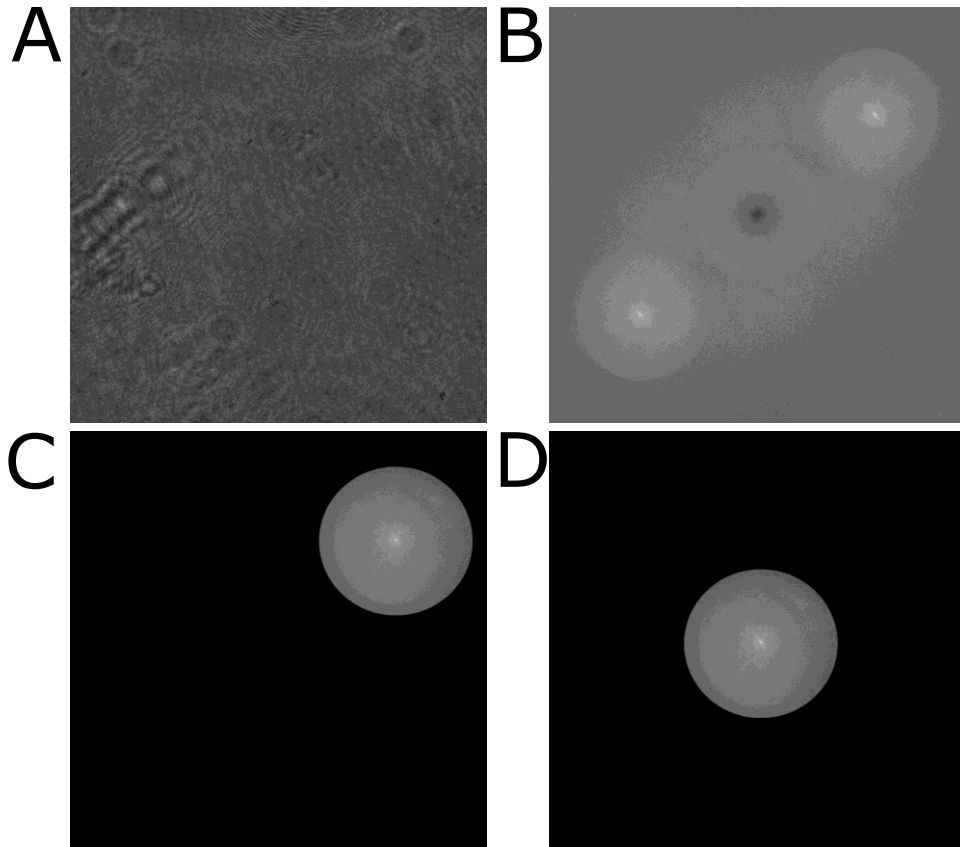


**Figure S1. The workflow for the initial processing of holographic data.** (A) A raw hologram. (B) The Fourier Transform of the raw hologram, plotted on a logarithmic scale. (C) The Fourier Transform of the hologram multiplied by a mask to isolate one of the high spatial frequency lobes. (D) The isolated lobe from (c) that has been linearly shifted to the center.

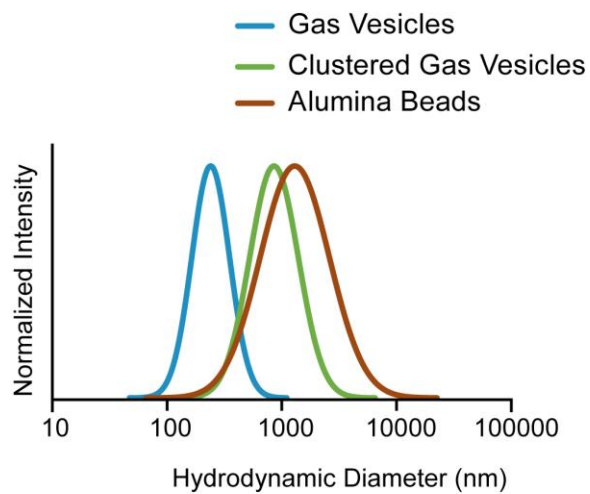


**Figure S2. Representative dynamic light scattering of the hydrodynamic diameter of pristine gas vesicles, clustered gas vesicles and alumina beads.**

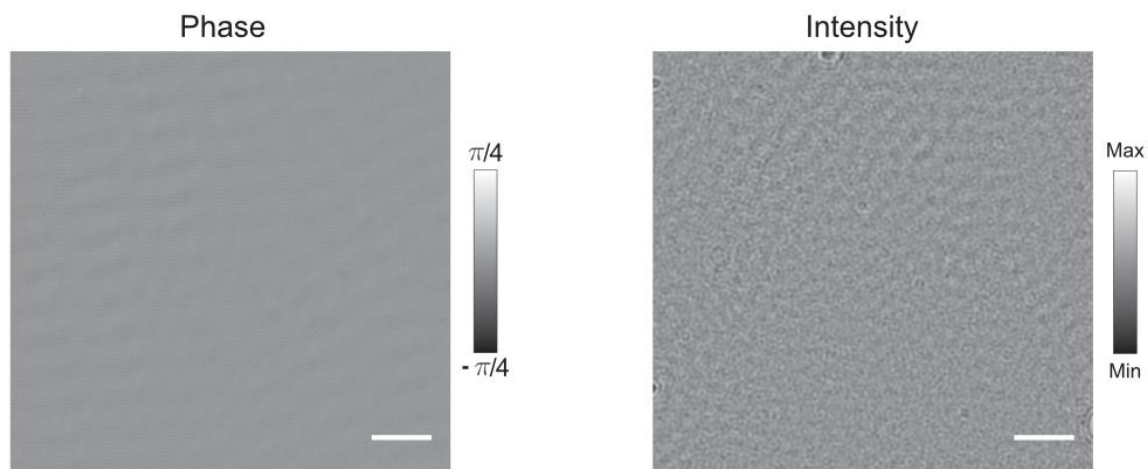


**Figure S3. Representative DHM phase and intensity images of clustered GVs collapsed using 1.2 MPa of hydrostatic pressure. Scale bar represents 25  $\mu\text{m}$ .**

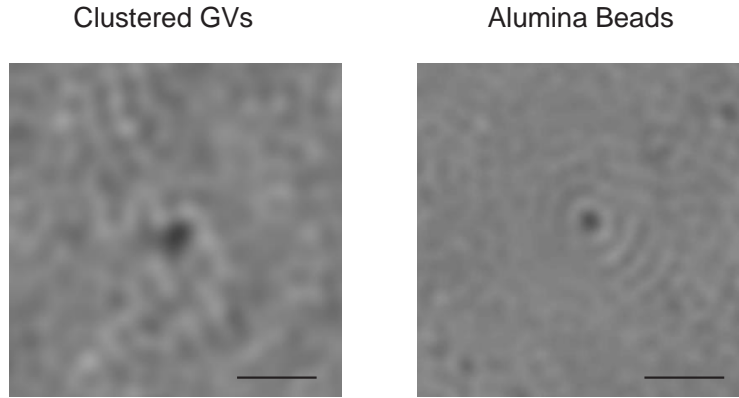


**Figure S4. Intensity images of the two particles from Figure 2K.** Scale bars represent 5 $\mu$ m.

**Table S1. Physical Properties of GV clusters, alumina beads, and water**

Property	GV Cluster (air)	Alumina	Water
Density (kg/m <sup>3</sup> )	1.2	2700	1000
Viscosity (N s/m <sup>2</sup> )	-	-	8.9 $\times$ 10 <sup>-4</sup>

### **Additional data sets**

The data for each supplement are in browsable directories at: Index of [ftp://131.215.99.205/Public/GVDHM\\_Data/](ftp://131.215.99.205/Public/GVDHM_Data/)

In addition to the browsable directories, there are pre-zipped packages of each of the supplements. The zipped packages can be unzipped with any software that will unzip 7z compressed files.

Connect as Guest (no password)

#### **Additional data set S1 (separate file)**

Raw holograms of GV clusters imaged with a coherent 405 nm laser

#### **Additional data set S2 (separate file)**

Raw holograms of alumina beads imaged with a coherent 405 nm laser

#### **Additional data set S3 (separate file)**

Raw holograms of GV clusters imaged in solution with a coherent 405 nm laser

#### **Additional data set S4 (separate file)**

Raw holograms of alumina beads imaged in solution with a coherent 405 nm laser

#### **Additional data set S5 (separate file)**

Raw holograms of GV clusters and alumina beads imaged in solution with a coherent 405 nm laser

#### **Additional data set S6 (separate file)**

Raw holograms of CHO cells with GV imaged with a coherent 405 nm laser

#### **Additional data set S7 (separate file)**

Raw holograms of GV expressing salmonella cells imaged with a coherent 405 nm laser

#### **Additional data set S8 (separate file)**

Raw holograms of GV expressing salmonella cells after GVs were hydrostatically collapsed. Imaged with a coherent 405 nm laser

#### **Additional data set S9 (separate file)**

MATLAB code of hologram simulation suite

## References

1. Kuhn, J.; Niraula, B.; Liewer, K.; Wallace, J. K.; Serabyn, E.; Graff, E.; Lindensmith, C.; Nadeau, J. L. *Rev Sci Instrum* **2014**, *85*, (12).
2. Lindensmith, C. A.; Rider, S.; Bedrossian, M.; Wallace, J. K.; Serabyn, E.; Showalter, G. M.; Deming, J. W.; Nadeau, J. L. *PLOS ONE* **2016**, *11*, (1), e0147700.
3. Wallace, J. K.; Rider, S.; Serabyn, E.; Kuhn, J.; Liewer, K.; Deming, J.; Showalter, G.; Lindensmith, C.; Nadeau, J. *Optics express* **2015**, *23*, (13), 17367-17378.
4. Lakshmanan, A.; Lu, G. J.; Farhadi, A.; Nety, S. P.; Kunth, M.; Lee-Gosselin, A.; Maresca, D.; Bourdeau, R. W.; Yin, M.; Yan, J.; Witte, C.; Malounda, D.; Foster, F. S.; Schroder, L.; Shapiro, M. G. *Nat Protoc* **2017**, *12*, (10), 2050-2080.
5. Lakshmanan, A.; Farhadi, A.; Nety, S. P.; Lee-Gosselin, A.; Bourdeau, R. W.; Maresca, D.; Shapiro, M. G. *ACS Nano* **2016**, *10*, (8), 7314-22.
6. Bourdeau, R. W.; Lee-Gosselin, A.; Lakshmanan, A.; Farhadi, A.; Kumar, S. R.; Nety, S. P.; Shapiro, M. G. *Nature* **2018**, *553*, (7686), 86-90.
7. Schnars, U.; Jüptner, W. P. *Measurement science and technology* **2002**, *13*, (9), R85.
8. Bedrossian, M.; Nadeau, J.; Serabyn, E.; Lindensmith, C. In *Sources and propagation of errors in quantitative phase imaging techniques using optical interferometry*, 2017, International Society for Optics and Photonics: p 100740E.
9. Schindelin, J.; Arganda-Carreras, I.; Frise, E.; Kaynig, V.; Longair, M.; Pietzsch, T.; Preibisch, S.; Rueden, C.; Saalfeld, S.; Schmid, B. *Nature methods* **2012**, *9*, (7), 676-682.